

**Revealing the correlation between real-space structure and chiral magnetic order at the atomic scale**Nadine Hauptmann,<sup>1</sup> Melanie Dupé,<sup>2</sup> Tzu-Chao Hung,<sup>1</sup> Alexander K. Lemmens,<sup>1</sup> Daniel Wegner,<sup>1</sup> Bertrand Dupé,<sup>2</sup> and Alexander A. Khajetoorians<sup>1,\*</sup><sup>1</sup>*Institute for Molecules and Materials, Radboud University, 6525 AJ Nijmegen, The Netherlands*<sup>2</sup>*Institut für Physik, Johannes Gutenberg Universität Mainz, D-55099 Mainz, Germany*

(Received 7 December 2017; published 9 March 2018)

We image simultaneously the geometric, the electronic, and the magnetic structures of a buckled iron bilayer film that exhibits chiral magnetic order. We achieve this by combining spin-polarized scanning tunneling microscopy and magnetic exchange force microscopy (SPEX) to independently characterize the geometric as well as the electronic and magnetic structures of nonflat surfaces. This new SPEX imaging technique reveals the geometric height corrugation of the reconstruction lines resulting from strong strain relaxation in the bilayer, enabling the decomposition of the real-space from the electronic structure at the atomic level and the correlation with the resultant spin-spiral ground state. By additionally utilizing adatom manipulation, we reveal the chiral magnetic ground state of portions of the unit cell that were not previously imaged with spin-polarized scanning tunneling microscopy alone. Using density functional theory, we investigate the structural and electronic properties of the reconstructed bilayer and identify the favorable stoichiometry regime in agreement with our experimental result.

DOI: [10.1103/PhysRevB.97.100401](https://doi.org/10.1103/PhysRevB.97.100401)

Chiral magnets, exhibiting magnetic skyrmions [1–4], have attracted much interest recently due to their potential application for nanoscale magnetic storage [5,6]. The dominating mechanism responsible for generating stable noncollinear configurations of the spin is the Dzyaloshinskii-Moriya interaction (DMI), which favors orthogonal configurations of the spin [7,8]. One key challenge for magnetic data storage is to generate isolated skyrmions with nanometer-scale sizes [9,10]. Tremendous effort has been made toward this end to stabilize isolated skyrmions at room temperature [5,11–13] or with length scales down to the nanometer scale at low temperatures, utilizing hybrid transition-metal interfaces to pin skyrmions at various types of defects [10]. In the latter case, the presence of isolated or arrays of defects raises the question how strong structural relaxations [14], such as surface reconstruction or buckling, simultaneously affect the various exchange interactions, geometric structures, and electronic properties, thus affect the magnetic order as well as the dynamics of chiral magnetic structures [15,16].

The most prevalent magnetic imaging technique that can access the magnetization of surfaces and interfaces at the atomic scale is spin-polarized scanning tunneling microscopy (SP-STM) [17]. Despite its overwhelming success over the past decade in characterizing surface and interfacial magnetism, SP-STM lacks the capability to solely detect either the topographic height profile or the magnetic structure as the tunneling current depends on the structural as well as the electronic and magnetic properties, which cannot easily be decomposed. In contrast, noncontact atomic force microscopy (NC-AFM) gives more accurate structural information as it is sensitive to the forces between the probe and the surface [18]. Combined with magnetic sensitivity, NC-AFM can probe the magnetic

exchange force at the atomic scale, referred to as magnetic exchange force microscopy (MExFM), yet it has been proven to be difficult to apply [19–22]. Up to now, there has been no demonstration of the combination of these methods to reveal the interplay between real-space and electronic structures and its effect on magnetic order at the atomic scale.

Here, we use the recently developed combination of SP-STM and MExFM (SPEX) [23] together with *ab initio* methods to deconvolute the real-space structure of a reconstructed bilayer of Fe on Ir(111) from the electronic and magnetic structures, which exhibit an atomic-scale spin-spiral ground state. We find that, in contrast to previous studies based solely on SP-STM [24], the larger height corrugation of the reconstruction lines as measured by NC-AFM is linked to a lower intensity spin-spiral structure in SP-STM. Furthermore, using a combination of SPEX and manipulation of adsorbed Fe adatoms, we address regions in the unit cell which were previously uncharacterized and extract the complete magnetic structure in relation to the geometric structure of the Fe bilayer. All these measurements provide an essential ingredient for *ab initio* calculations of such complex structures, and by considering various stoichiometries we explain the reconstruction of the Fe bilayer.

Fe layers and single Fe adatoms were deposited *in situ* on an Ir(111) surface cleaned in UHV and subsequently characterized with an STM/AFM based on the qPlus tuning fork method [25] (PtIr or Fe tips) at  $T = 6.3$  K (see the Supplemental Material [26]). We performed density functional theory (DFT) calculations using the Vienna *ab initio* simulation package [27–30]. We employed projector augmented plane waves [31,32] with the generalized gradient approximation exchange-correlation functional in the parametrization of Perdew-Burke-Ernzerhof [33]. As cutoff energy of the plane waves 300 eV was chosen, a  $\Gamma$ -centered Monkhorst-Pack mesh [34] of  $1 \times 5 \times 1$   $k$  points was used containing three  $k$  points in the irreducible part of the

\*Corresponding author: [a.khajetoorians@science.ru.nl](mailto:a.khajetoorians@science.ru.nl)

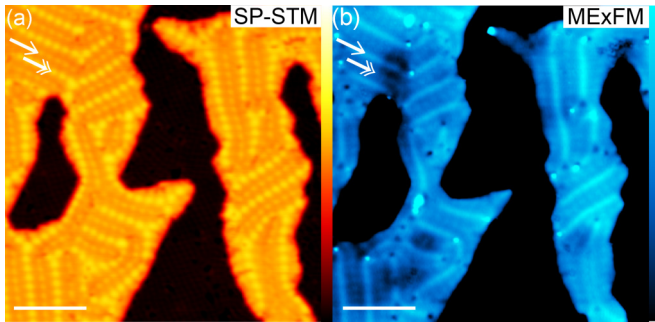


FIG. 1. (a) Large-scale constant current SP-STM image ( $V_s = 50$  mV,  $I_T = 100$  pA, Fe tip) and constant frequency shift MExFM image ( $\Delta f_{\text{set}} = -12$  Hz,  $z_{\text{mod}} = 100$  pm, and  $V_s = 0.1$  mV, Fe tip). Both images:  $43.5 \times 43.5$  nm<sup>2</sup>. Scale bars are 10 nm. Color scales are (a) 0.4–500 pm and (b) 220–240 pm.

Brillouin zone for the  $9 \times 1 \times 1$  supercell in the orthorhombic setting, which contains 18 Ir atoms per substrate layer. The in-plane lattice constant was kept constant at 2.70 Å. The two Fe layers were allowed to relax until residual forces were smaller than 0.01 eV/Å, whereas the positions of the Ir atoms were kept fixed (see the Supplemental Material [26]). Magnetic moments were initialized in the ferromagnetic order. The crystal structures were visualized using the software VESTA [35].

Figure 1 illustrates a characterization of the bilayer Fe on Ir(111) utilizing SPEX imaging, which exhibits a periodic network of reconstruction lines (RLs). This network has been described in a recent work to originate from uniaxial strain relief between the pseudomorphically grown first Fe layer and the second-layer Fe atoms [24]. This RL network hosts a spin-spiral texture and forms 120° rotational domains as detailed by magnetic-field-dependent measurements in Ref. [24]. The SP-STM image [Fig. 1(a)], acquired with an Fe bulk tip sensitive to the out-of-plane magnetization, shows RLs with lower (dark) and higher (bright) intensities, marked by a single- and a double-headed arrow, respectively. The typical spacing between two bright RLs is  $3.3 \pm 0.2$  nm, which is smaller than the recently reported spacing of 5.2 nm [24]. Along the bright and dark RLs, bright protrusions with a periodicity of  $1.24 \pm 0.05$  nm are observed, which correspond to the out-of-plane magnetic moments of the cycloidal spin spiral that runs along the RL [24]. We note that the appearance of the spin contrast of the spin spirals strongly depends on the bias voltage (see the Supplemental Material [26]).

The MExFM image in constant frequency shift mode [Fig. 1(b)] gives more insight into the height corrugation derived from the RLs. The total force between the Fe bulk tip and the surface responsible for the image contrast consists of various force contributions, which are long- and short-range magnetic forces, van der Waals forces, as well as short-range chemical forces. We exclude local contributions from electrostatic forces due to the metallic substrate. The arrows in Fig. 1(b) mark the same location of the bright and dark RLs as in Fig. 1(a). Interestingly, the dark RL in the SP-STM image corresponds to a brighter contrast in the MExFM image, which we interpret as a height corrugation of the Fe bilayer. Likewise, the bright RL in the SP-STM image corresponds to a smaller

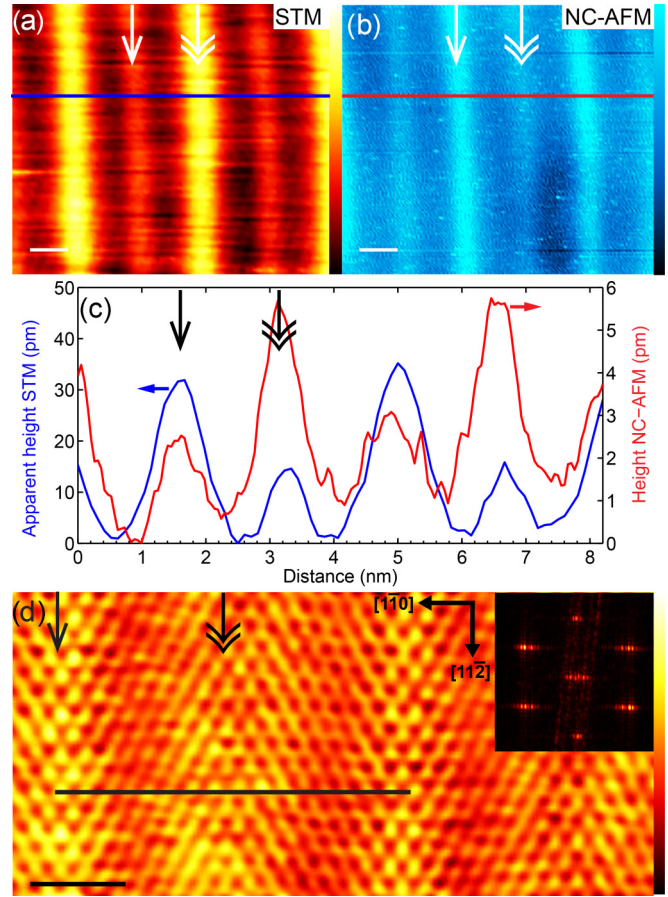


FIG. 2. (a) Constant-current STM ( $V_s = 50$  mV,  $I_T = 100$  pA, PtIr tip) and constant frequency shift NC-AFM images (flattened by an offset,  $\Delta f_{\text{set}} = -40$  Hz,  $z_{\text{mod}} = 100$  pm, and  $V_s = 0.1$  mV). (c) Line profiles of the STM and NC-AFM images along the horizontal lines as indicated in (a) and (b). The NC-AFM has been smoothed prior to taking the line profile by a Gaussian filter with two points. (d) Atomic resolution STM image (flattened by an offset, Gaussian smoothed by two points,  $V_s = 1$  mV,  $I_T = 48$  nA, PtIr tip) and the inset shows the fast Fourier transform (FFT) of (d). Sizes: (a)  $8.5 \times 7.3$  nm<sup>2</sup>, (b)  $8.5 \times 7.3$  nm<sup>2</sup>, and (d)  $6.8 \times 3.3$  nm<sup>2</sup>. Scale bars are 1 nm for all images. Color scales are (a) 0–54 pm, (b) 1–11 pm, and (d) 0–28 pm. The arrows indicate equivalent positions in all images.

corrugation in the MExFM image. This is counterintuitive and shows that the electronic/magnetic and topographic structures of the bilayer are all strongly convoluted in SP-STM and that it is not possible to unambiguously extract the exact geometric structure from SP-STM alone.

Next, we focus on the vertical relaxations resulting from the RLs. In order to exclude magnetic contributions, we used a nonmagnetic PtIr tip attached to the qPlus sensor. Figures 2(a) and 2(b) show STM and NC-AFM images, respectively, of a closeup view of one RL domain. In agreement with the data acquired with the magnetic Fe tip (Fig. 1), a RL with a larger apparent height in the constant current STM image [Fig. 2(a)] corresponds to a smaller corrugation in the NC-AFM image [Fig. 2(b)] and vice versa (indicated by the single- and double-headed arrows). From line profiles [Fig. 2(c)] we extract  $4.7 \pm 1$  pm for the larger and  $2.2 \pm 1$  pm for the smaller

height corrugation in NC-AFM images, respectively. The given error margins include uncertainties of the piezoconstants, the noise extracted from raw data line profiles of NC-AFM images, as well as the variation of the corrugation values for different reconstruction lines. Compared to that, the apparent-height corrugation in the STM image is about one order of magnitude larger than in the NC-AFM image. These findings from combined STM and NC-AFM images indicate that the film exhibits strong vertical relaxations within the unit cell, and thus the Fe film cannot be considered flat [10] necessitating the characterization of SPEX imaging for such strongly relaxed surfaces.

By bringing the PtIr tip closer to the surface, we resolve the previously uncharacterized atomic lattice utilizing constant-current STM imaging [Fig. 2(d)]. The atomic lattice spacing in the  $[1\bar{1}0]$  direction varies between 2.0 and 2.7 Å as indicated by the elongated spots of the FFT (the inset). We further find that the atomic lines along the  $[1\bar{1}0]$  direction do not form rows but rather exhibit a pattern reminiscent of thin transition-metal films [36–38], which can be seen by following the atom positions (bright spots) along the horizontal line in Fig. 2(d). Along this line we extract that 16 atoms are located between the two dark RLs. The Fe atoms in the first layer grow pseudomorphically on the Ir(111) atomic lattice with a nearest-atom spacing [39] of 2.72 Å. Considering the spacing of the RLs ( $3.3 \pm 0.2$  nm) we extract a compression along the  $[1\bar{1}0]$  direction between 7% and 8% in the Fe bilayer. This is comparable with the compression for the previously suggested model of the atomic arrangement in the Fe bilayer where a variation of the atom stacking among fcc, hcp, and bcc areas has been suggested and a compression of 5% to 6% has been stated [24]. However, the RL network in our Rapid Communication deviates from recent findings: First, the spacing in between the RLs is smaller in our Rapid Communication. This might be a consequence of different film preparation procedures as described in the Supplemental Material in Ref. [26]. Second, from NC-AFM and MExFM images we extract a height corrugation up to 5 pm, which has not been described in the previous work in which the structure was considered to be planar. Using SPEX imaging, we can obtain complementary information, which provides direct information on the vertical relaxation for strained film structures providing necessary input for *ab initio* methods.

In Fig. 3(a), a simulated STM image is presented along with the atomic structure of the reconstructed overstoichiometric (10:9) surface, which is energetically the most favorable. In total, we calculated reconstruction energies of five different surface structures of which two form a reconstructed domain pattern and the remaining three are pseudomorphic homogeneous surfaces with bcc-like stacking as well as fcc and hcp stackings of the Fe (top) layer (see the Supplemental Material [26]). The STM image [Fig. 3(a)] was obtained from the electron density calculated 100 pm above the surface layer arising from the electronic states at the Fermi energy, which is proportional to STM current intensities. The Fe (top) atoms at the surface form a periodic structure (orange atoms) where two differently oriented bcc domains are tilted against each other and twisted with respect to the Fe (bottom) layer (blue atoms). As a consequence, the atomic rows are not straight but follow a

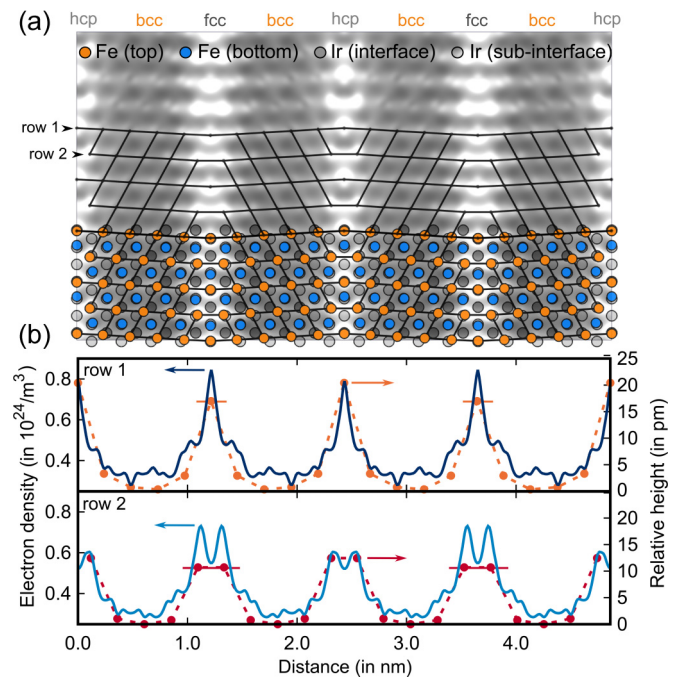


FIG. 3. Characterization of the reconstructed overstoichiometric (10:9) surface from *ab initio* supercell calculations. In (a), a simulated STM image is presented along with the atomic structure of the reconstructed surface. In (b), a more detailed analysis of the atomic and electronic structures along the two atomic rows indicated in (a) is given.

zigzag pattern as indicated in Fig. 3(a). The domain boundaries are formed by lines of surface atoms Fe (top) possessing fcc or hcp stacking, which appear bright in the STM image, whereas the interior of the bcc domains appears dark.

Figure 3(b) shows a more detailed analysis of the atomic and electronic structures along the two atomic rows indicated in (a). The relative heights of the Fe (top) atoms are shown in orange and red. The reconstructed surface exhibits a strong buckling with two different types of maxima in both RLs: hcp atoms are higher than fcc atoms by up to 3.4 pm. In the blue colors, the electron densities along the same rows obtained at a height of 100 pm above the surface (as in the simulated STM image) are given. Counterintuitively, the higher hcp regions at distances of 0.0, 2.4, and 4.8 nm possess lower electron densities than the lower fcc regions at distances of 1.2 and 3.6 nm. The higher hcp RLs appear slightly darker in the STM image than the lower fcc RLs. The low-lying atoms within the bcc domains appear darkest. Altogether, our simulated STM image of the overstoichiometric (10:9) surface agrees well with the findings from atomically resolved STM as well as combined STM/NC-AFM images (Fig. 2). In particular, the existence of hcp and fcc RLs with different geometrical heights will have consequences for the magnetic structure as the DMI is strongly dependent on the surface geometry. Our results also show that STM imaging alone cannot reveal the real-space structure as it convolutes the electronic structure and the surface relaxation. In contrast, NC-AFM can reveal the real-space structure independent of the surface electron density which is essential for consideration of complex magnetic structures [10].

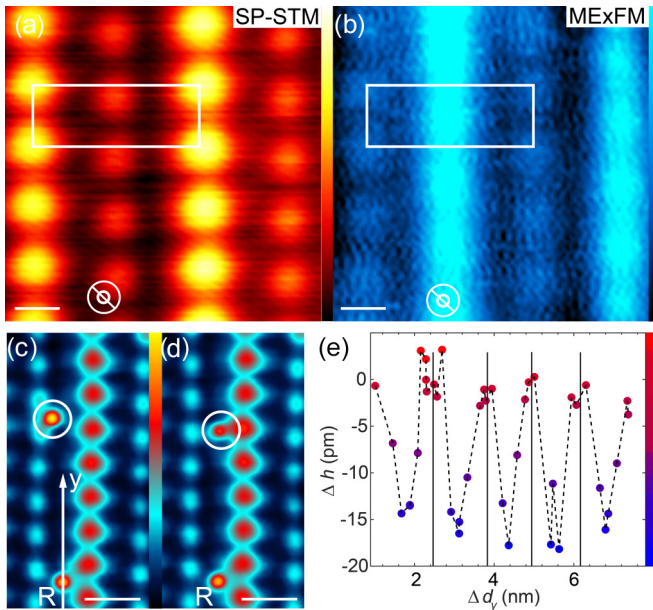


FIG. 4. (a) Constant-current SP-STM ( $V_s=50$  mV,  $I_T=100$  pA, Fe tip) and constant frequency shift MExFM image (flattened by an offset, smoothed by a Gaussian filter with two points,  $\Delta f_{\text{set}} = -19$  Hz,  $z_{\text{mod}} = 100$  pm, and  $V_s = 0.0$  mV, Fe tip). Scale bars are 1 nm. The tip magnetization is out of plane as indicated by the symbol. (c) and (d) Constant-current SP-STM images (Fe tip,  $V_s = 50$  mV,  $I_T = 100$  pA, smoothed by Gaussian filter two points); scale bars are 2 nm. Color bar: (a) 0–56 pm; (b) 0–5 pm; (c) and (d): 0–76 pm. The Fe adatom (the white circle) was moved in between the dark and the bright spin spirals. The reference atom  $R$  rests at the same position (see the Supplemental Material [26]). (e) Apparent height  $\Delta h$  of the adatom versus the distance  $\Delta d_j$  to the reference atom  $R$  when moved along a line in between the dark and the bright spin spirals. The  $y$  direction is defined in (c).

We note that the observed domain width (and bilayer stoichiometry) is determined by the supercell size, which is limited by computational cost. Thus, different periodicity lengths of the domain structure are possible and depend presumably crucially on the preparation conditions of the bilayer as evidenced by the different RL spacings found in our and the previous work (see the Supplemental Material [26]). The main features of the reconstructed surface structures, however, will remain unchanged: (1) prevalence of bcc domains and (2) tilt-domain boundaries formed by fcc and hcp atoms resulting in pronounced buckling of the surface layer.

Now that the structural model has been established, we finally analyze the magnetic structure of the Fe bilayer using SPEX in combination with single adatom manipulation to characterize regions of the unit cell previously uncharacterized. A closeup view of one domain of the spin-spiral network is shown in Figs. 4(a) and 4(b). The SP-STM image agrees with previous measurements [24]. In addition, however, we also observe the spin spiral in the MExFM image, which can be clearly discerned on the RLs with the lower corrugation and is resolvable on the RLs with larger corrugation as also seen in the overview MExFM image in Fig. 1. Although the SPEX images reveal the out-of-plane magnetization on the RLs, we cannot

conclude what the magnetization of the atoms between the RLs is due to the inherent topographic and electronic contrast variations. Therefore, we utilize a deposited Fe adatom and manipulate its position with respect to the surface magnetic unit cell to infer the magnetization (see the Supplemental Material [26] and Ref. [40]). This is performed in the following manner: (1) additional Fe adatoms are evaporated onto the surface and (2) one adatom is manipulated along a row in between a dark and a bright RLs, and the changes in spin contrast between the moved adatom and a reference adatom (remaining at a fixed position) is compared. We presume that the deposited adatoms are strongly exchange coupled to the surface and electronically equivalent. Therefore, their intensity reflects the change in the magnetic state of the underlying spin spiral without strongly perturbing the underlying magnetic state as long as the coverage is dilute. Figures 4(c) and 4(d) show SP-STM images of an Fe adatom (white circles) that has been manipulated in between the area of bright and dark RLs. We reproducibly moved an individual Fe adatom over about 100 different positions (see the Supplemental Material [26]). As seen from Figs. 4(c) and 4(d), the apparent height of the Fe adatom varies depending on the position.

To systematically investigate the apparent-height variation of the Fe adatom, we consider the apparent-height difference  $\Delta h$  between the Fe adatom and the reference Fe adatom ( $R$ ) whose apparent height does not change during the entire manipulation process. Figure 4(e) shows the dependence of  $\Delta h$  along the  $y$  direction [as defined in Fig. 4(c)]. The apparent height oscillates at different positions along the  $y$  direction with the same periodicity as the spin spiral (between 1.2 and 1.3 nm). As can be seen from Figs. 4(c) and 4(d), the apparent-height variation of the Fe adatom is phase shifted by  $180^\circ$  with respect to the contrast of the spin spiral. Along the direction orthogonal to the  $y$  direction,  $\Delta h$  does not vary significantly (see the Supplemental Material [26]).

We conclude from our data that the out-of-plane magnetic moment of the adatom alternates along the  $[11\bar{2}]$  direction whereas the variation along the  $[1\bar{1}0]$  is small. Our observation is in agreement with a previously suggested magnetic structure [24] if we assume that the Fe adatom exhibits an inversion of the spin polarization with respect to the underlying Fe bilayer [41,42].

To summarize, we used the new SPEX imaging technique together with *ab initio* DFT calculations to experimentally delineate the interplay between surface reconstruction and magnetic structure of the spin-spiral network in Fe bilayers on Ir(111). We show that the reconstruction lines are subject to a substantial vertical corrugation ( $\Delta z \approx 5$  pm), resulting from the energetically favorable overstoichiometric surface, which we measured by NC-AFM and confirmed using DFT. Our results illustrate that strong relaxation effects due to defects or strain cannot be extracted from SP-STM measurements alone and may be an important consideration for *ab initio* calculations of the magnetic structure as well as in thin magnetic films [10]. These strong structural relaxations may have an important effect on the exchange interactions and potentially on the DMI that stabilize the magnetic texture of the bilayer by modifying the interfacial hybridization and therefore require careful consideration.

We would like to thank K. von Bergmann, A. Kubetzka, J. Sinova, and S. Heinze for useful discussions. We would like to acknowledge financial support from the Emmy Noether Program (Grant No. KH324/1-1) via the Deutsche Forschungsgemeinschaft, and the Foundation of Fundamental Research on Matter (FOM), which is part of the Netherlands Organization for Scientific Research (NWO), and the VIDI Project: “Manipulating the interplay between superconductivity and chiral magnetism at the single atom level” with Project No.

680-47-534 which is financed by the NWO. N.H. and A.A.K. also acknowledge support from the Alexander von Humboldt Foundation via the Feodor Lynen Research Fellowship. M.D. and B.D. gratefully acknowledge the computing time granted on the supercomputer Mogon at Johannes Gutenberg University Mainz [43]. B.D. and M.D. also acknowledge financial support from the Alexander von Humboldt Foundation and the Transregional Collaborative Research Center SFB/TRR 173 “Spin+X” from the Deutsche Forschungsgemeinschaft.

- 
- [1] A. N. Bogdanov and D. A. Yablonskii, *Zh. Eksp. Teor. Fiz.* **95**, 178 (1989) [*JETP* **68**, 101 (1989)].
- [2] S. Mühlbauer, B. Binz, F. Jonietz, C. Pfleiderer, A. Rosch, A. Neubauer, R. Georgii, and P. Böni, *Science* **323**, 915 (2009).
- [3] X. Z. Yu, Y. Onose, N. Kanazawa, J. H. Park, J. H. Han, Y. Matsui, N. Nagaosa, and Y. Tokura, *Nature (London)* **465**, 901 (2010).
- [4] F. Jonietz, S. Mühlbauer, C. Pfleiderer, A. Neubauer, W. Münzer, A. Bauer, T. Adams, R. Georgii, P. Böni, R. A. Duine, K. Everschor, M. Garst, and A. Rosch, *Science* **330**, 1648 (2010).
- [5] W. Jiang, P. Upadhyaya, W. Zhang, G. Yu, M. B. Jungfleisch, F. Y. Fradin, J. E. Pearson, Y. Tserkovnyak, K. L. Wang, O. Heinonen, S. G. E. te Velthuis, and A. Hoffmann, *Science* **349**, 283 (2015).
- [6] J. Sampaio, V. Cros, S. Rohart, A. Thiaville, and A. Fert, *Nat. Nanotechnol.* **8**, 839 (2013).
- [7] T. Moriya, *Phys. Rev.* **120**, 91 (1960).
- [8] I. E. Dzialoshinskii, *Zh. Eksp. Teor. Fiz.* **32**, 1547 (1957) [*Sov. Phys. JETP* **5**, 1259 (1957)].
- [9] N. Romming, C. Hanneken, M. Menzel, J. E. Bickel, B. Wolter, K. von Bergmann, A. Kubetzka, and R. Wiesendanger, *Science* **341**, 636 (2013).
- [10] P.-J. Hsu, A. Kubetzka, A. Finco, N. Romming, K. von Bergmann, and R. Wiesendanger, *Nat. Nanotechnol.* **12**, 123 (2017).
- [11] C. Moreau-Luchaire, C. Moutafis, N. Reyren, J. Sampaio, C. A. F. Vaz, N. Van Horne, K. Bouzehouane, K. Garcia, C. Deranlot, P. Warnicke, P. Wohlhüter, J. M. George, M. Weigand, J. Raabe, V. Cros, and A. Fert, *Nat. Nanotechnol.* **11**, 444 (2016).
- [12] A. Fert, V. Cros, and J. Sampaio, *Nat. Nanotechnol.* **8**, 152 (2013).
- [13] S. Woo, K. Litzius, B. Krüger, M.-Y. Im, L. Caretta, K. Richter, M. Mann, A. Krone, R. M. Reeve, M. Weigand, P. Agrawal, I. Lemesch, M.-A. Mawass, P. Fischer, M. Kläui, and G. S. D. Beach, *Nat. Mater.* **15**, 501 (2016).
- [14] C. Hanneken, A. Kubetzka, K. von Bergmann, and R. Wiesendanger, *New J. Phys.* **18**, 055009 (2016).
- [15] W. Legrand, D. Maccariello, N. Reyren, K. Garcia, C. Moutafis, C. Moreau-Luchaire, S. Collin, K. Bouzehouane, V. Cros, and A. Fert, *Nano Lett.* **17**, 2703 (2017).
- [16] J.-V. Kim and M.-W. Yoo, *Appl. Phys. Lett.* **110**, 132404 (2017).
- [17] M. Bode, M. Heide, K. von Bergmann, P. Ferriani, S. Heinze, G. Bihlmayer, A. Kubetzka, O. Pietzsch, S. Blugel, and R. Wiesendanger, *Nature (London)* **447**, 190 (2007).
- [18] F. J. Giessibl, *Rev. Mod. Phys.* **75**, 949 (2003).
- [19] R. Schmidt, C. Lazo, H. Hölscher, U. H. Pi, V. Caciuc, A. Schwarz, R. Wiesendanger, and S. Heinze, *Nano Lett.* **9**, 200 (2009).
- [20] U. Kaiser, A. Schwarz, and R. Wiesendanger, *Nature (London)* **446**, 522 (2007).
- [21] F. Pielmeier and F. J. Giessibl, *Phys. Rev. Lett.* **110**, 266101 (2013).
- [22] J. Grenz, A. Köhler, A. Schwarz, and R. Wiesendanger, *Phys. Rev. Lett.* **119**, 047205 (2017).
- [23] N. Hauptmann, J. Gerritsen, D. Wegner, and A. A. Khajetoorians, *Nano Lett.* **17**, 5660 (2017).
- [24] P.-J. Hsu, A. Finco, L. Schmidt, A. Kubetzka, K. von Bergmann, and R. Wiesendanger, *Phys. Rev. Lett.* **116**, 017201 (2016).
- [25] F. J. Giessibl, *Appl. Phys. Lett.* **73**, 3956 (1998).
- [26] See Supplemental Material at <http://link.aps.org/supplemental/10.1103/PhysRevB.97.100401> for experimental details, large-scale and voltage-dependent SP-STM images, constant height images, Fe adatom manipulation, analysis of the periodicity of the spin spirals, voltage-dependent SPEX images, and details of the *ab initio* calculations.
- [27] G. Kresse and J. Hafner, *Phys. Rev. B* **47**, 558 (1993).
- [28] G. Kresse and J. Hafner, *Phys. Rev. B* **49**, 14251 (1994).
- [29] G. Kresse and J. Furthmüller, *Phys. Rev. B* **54**, 11169 (1996).
- [30] G. Kresse and J. Furthmüller, *Comput. Mater. Sci.* **6**, 15 (1996).
- [31] G. Kresse and D. Joubert, *Phys. Rev. B* **59**, 1758 (1999).
- [32] P. E. Blöchl, *Phys. Rev. B* **50**, 17953 (1994).
- [33] J. P. Perdew, K. Burke, and M. Ernzerhof, *Phys. Rev. Lett.* **77**, 3865 (1996).
- [34] H. J. Monkhorst and J. D. Pack, *Phys. Rev. B* **13**, 5188 (1976).
- [35] K. Momma and F. Izumi, *J. Appl. Crystallogr.* **44**, 1272 (2011).
- [36] J. Hrbek, J. de la Figuera, K. Pohl, T. Jirsak, J. A. Rodriguez, A. K. Schmid, N. C. Bartelt, and R. Q. Hwang, *J. Phys. Chem. B* **103**, 10557 (1999).
- [37] G. O. Pötschke and R. J. Behm, *Phys. Rev. B* **44**, 1442 (1991).
- [38] H. Brune, H. Röder, C. Boragno, and K. Kern, *Phys. Rev. B* **49**, 2997 (1994).
- [39] S. Heinze, K. von Bergmann, M. Menzel, J. Brede, A. Kubetzka, R. Wiesendanger, G. Bihlmayer, and S. Blügel, *Nat. Phys.* **7**, 713 (2011).
- [40] D. Serrate, P. Ferriani, Y. Yoshida, S.-W. Hla, M. Menzel, K. von Bergmann, S. Heinze, A. Kubetzka, and R. Wiesendanger, *Nat. Nanotechnol.* **5**, 350 (2010).
- [41] L. H. Zhou, F. Meier, J. Wiebe, and R. Wiesendanger, *Phys. Rev. B* **82**, 012409 (2010).
- [42] P. Ferriani, C. Lazo, and S. Heinze, *Phys. Rev. B* **82**, 054411 (2010).
- [43] <https://hpc.uni-mainz.de>.